

# Interaction of iron-nickel alloys with liquid aluminium

## Part II *Formation of intermetallics*

V. I. DYBKOV

*Institut Problem Materialoznavstva, Kyiv 03180, Ukraine*

*E-mail: dep6@materials.kiev.ua*

The phase composition of the one-phase intermetallic layer(s) and two-phase reaction zone(s) at the interface between a solid iron-nickel alloy, containing 90, 75, 50, 25, 20, 15 and 10 mass% Fe, and the aluminium melt, saturated with alloy constituents at 700°C, was studied by electron probe microanalysis. The formation of binary ( $\text{FeAl}_3$ ,  $\text{Fe}_2\text{Al}_7$ ,  $\text{NiAl}_3$  and surprisingly  $\text{NiAl}_2$  rather than  $\text{Ni}_2\text{Al}_3$ ) and ternary ( $\text{FeNiAl}_9$ ) intermetallic compounds was observed. All the binaries were found to dissolve considerable amounts of a third element (Ni or Fe) and to have a noticeable range of homogeneity. Dissolution of the Fe-Ni alloy base into pure liquid aluminium resulted in a large decrease (three to five times) of the layer thickness compared to the case of the saturated melt. © 2000 Kluwer Academic Publishers

### 1. Introduction

In contrast to binary systems where only one-phase intermetallic layers can occur at the interface between initial elementary substances, in ternary systems, when a two-component alloy reacts with a third metal (either solid or liquid), the formation of both compact one-phase layers and two-phase reaction zones is possible. When investigating the layer-growth kinetics at the solid-liquid interface, it is essential either to take account of the effect of dissolution on the layer formation or to exclude its influence at all by means of prior saturation of the liquid metal with alloy constituents.

Part I of this paper was devoted to the study of the dissolution kinetics of iron-nickel alloys in liquid aluminium [1]. Aluminium is known to form a number of intermetallics with iron and nickel, both binary [2–4] and ternary [5–7]. In Part II, the intermetallic compound formation at the interface between a solid iron-nickel alloy, containing 90, 75, 50, 25, 20, 15 and 10 mass% Fe, and the aluminium melt, saturated with alloy constituents at 700°C, will be described. Also, the effect of dissolution on the process of layer growth will be illustrated.

### 2. Experimental procedure

#### 2.1. Materials and alloy preparation

High-purity aluminium (99.995 mass% Al), carbonyl iron (99.98 mass% Fe) and electrolytic-grade nickel (99.98 mass% Ni) were used for this investigation. The Fe-Ni alloys were prepared from their components in a conventional arc-melting furnace under argon and then cast into a 13 mm inner diameter (i.d.) and 100 mm high massive copper crucibles. By inverting the ingots between melts and remelting five times, homogeneous alloys could readily be obtained.

#### 2.2. Fe-Ni specimens

Cylindrical specimens,  $11.28 \pm 0.01$  mm diameter and 6 mm high, were machined from the 13 mm diameter Fe-Ni alloy rods. The disc surfaces were then ground flat and polished mechanically.

Before the experiment, the alloy specimen was rinsed in ethonol and dried. Then, it was pressed into a 16 mm diameter high-purity graphite tube to protect its lateral surface from the liquid-metal attack. Therefore, only the disc surface, 1 cm<sup>2</sup> area, contacted with the aluminium melt during the run.

Chemical compositions of the Fe-Ni specimens corresponded to nominal values (within  $\pm 0.5$  mass%) [1]. At room temperature the alloy specimens consisted of the  $\alpha$ -phase (ferrite) at nickel contents less than or equal to 25 mass% or the  $\gamma$ -phase (austenite) at higher Ni contents, while at the temperature chosen in this investigation, 700°C, the specimens of all compositions had austenitic structures [1].

#### 2.3. Methods

The experiments were carried out mainly by the rotating disc technique. A schematic diagram to illustrate the run is shown in Fig. 1.

A flux was used both to protect the aluminium melt from oxidation and to pre-heat the Fe-Ni specimen to the required temperature. The flux was first melted in a 26 mm i.d. alumina crucible. Its melting began at approximately 350°C. Then, pieces of aluminium (24 g) were melted under a flux. At a temperature of about 700°C, the appropriate amount of Fe-Ni alloy shavings corresponded to the saturation concentration [1] was added to aluminium, with subsequent temperature raising up to 800°C. After a 30 min holding at that

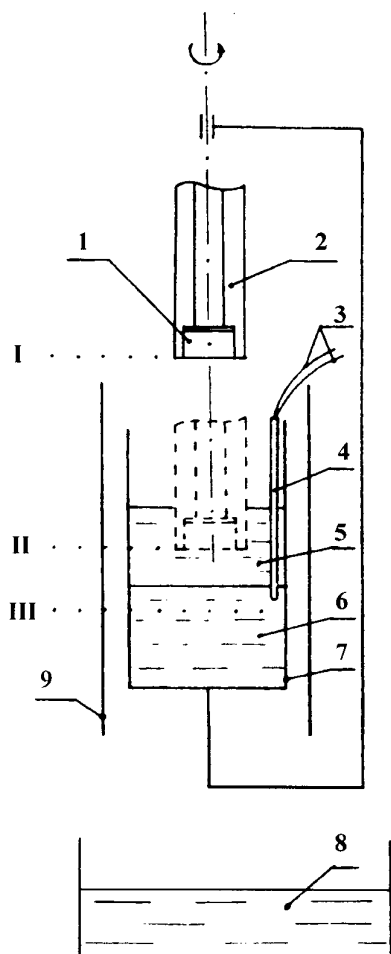


Figure 1 Schematic diagram to illustrate the experiment. 1, Fe-Ni alloy specimen; 2, graphite protective tube (holder); 3, chromel-alumel thermocouple; 4, alumina protective sheath; 5, molten flux; 6, aluminium melt; 7, alumina crucible; 8, water bath; 9, electrical furnace.

temperature, Fe-Ni alloy shavings fully dissolved in liquid aluminium. The aluminium melt was then cooled down to a temperature of  $720^{\circ}\text{C}$ , and the Fe-Ni specimen, rotating at an angular speed of  $6.45 \text{ rad sec}^{-1}$ , was lowered from position I into position II (see Fig. 1). During pre-heating, the distance between the disc surface and the melt one was around 10 mm. When the temperature had equilibrated at  $700^{\circ}\text{C}$  (typically after 500 sec), the Fe-Ni specimen was lowered from position II into position III in the bulk of the aluminium melt, so that the distance between the disc surface and the crucible bottom was  $15 \pm 0.5 \text{ mm}$ . That was the beginning of the run.

The temperature of the liquid phase was measured by a chromel-alumel thermocouple. Its deviation from the required value  $700^{\circ}\text{C}$  did not exceed  $\pm 2^{\circ}\text{C}$ .

After holding the Fe-Ni specimen in the aluminium melt for a pre-determined period of time, the crucible, together with the flux, the melt and the specimen, was immersed into water to arrest the reactions at the alloy-aluminium interface. The time of cooling from the experiment temperature to a temperature of solidification of the aluminium melt was 15–20 sec, while that of further cooling to room temperature was 10–15 sec (about 30 sec in total). Such a relatively low cooling rate allowed spluttering the melt to be avoided.

To illustrate the influence of dissolution on the layer-growth rate, two sets of experiments were carried out at  $700^{\circ}\text{C}$  and a dipping time of 900 sec. In the first set, the saturated aluminium melts were used. In the second, the pure liquid aluminium was employed. In the latter case, the Fe-Ni disc specimen was rotated in the liquid phase at an angular speed of  $24.0 \text{ rad sec}^{-1}$ .

After cooling to room temperature, the Al/(Fe-Ni) specimen obtained was cut along the cylindrical axis, ground flat and polished electrolytically. The cross-sections prepared in such a way were examined metallographically. Aluminium, iron and nickel contents in the transition zone between the interacting phases were found by electron probe microanalysis (EPMA) using a JEOL Superprobe 733 microanalyser operating at 25 kV and a CAMECA Camebax SX50 microanalyser operating at 15 kV. The spot diameter and the phase volume analysed at each point were estimated to be  $1.5 \text{ to } 2 \mu\text{m}$  and  $2 \text{ to } 3 \mu\text{m}^3$ , respectively. Therefore, the composition of intermetallic layers whose thickness exceeded  $5 \mu\text{m}$  could be measured reliably. In most cases, measurements were repeated on the same specimen with the help of another microanalyser to avoid possible systematic instrumental errors. Both sets of the data thus obtained always coincided fairly well.

Microhardness measurements were also carried out using a conventional tester with the diamond pyramid. The load was 0.49 N (50 g).

### 3. Results and discussion

#### 3.1. Al-Fe-Ni equilibrium phase diagram

The equilibrium phase diagram is helpful in analysing the process of intermetallic layer formation at the interface between iron-nickel alloys and aluminium melts. Projection of the liquidus surface on the concentration triangle and distribution of the phase fields in the solid state for Al-rich Al-Fe-Ni alloys are shown in Fig. 2.

The Al-richest Al-Fe binary phase is designated as  $\text{FeAl}_3$  (25.0 at% Fe, 75.0 at% Ni) or  $\text{Fe}_2\text{Al}_7$  (22.2 at% Fe, 77.8 at% Ni) [1, 5]. Yet, it is debatable whether these intermetallic compounds are two different phases or the same phase with a wide range of homogeneity. The  $\text{FeAl}_3$  compound is reported to have a homogeneity range of 74.5 to 75.5 at% Al [7]. The range of homogeneity of the  $\text{Fe}_2\text{Al}_7$  compound is indicated as 77.5 to 78.6 at% Al [1]. The X-ray powder pattern of  $\text{FeAl}_3$  was found to be only slightly different from that of  $\text{Fe}_2\text{Al}_7$  [1]. Up to 11 at% Ni may be dissolved in  $\text{FeAl}_3$  [7].

In the Al-Ni binary system, the homogeneity range of  $\text{Ni}_2\text{Al}_3$  (ideal chemical composition 40 at% Ni, 60 at% Al) is given as 59.2 to 63.7 [1] or 58.5 to 63.0 at% Al [7], whereas that of  $\text{NiAl}_3$  (25.0 at% Ni, 75.0 at% Al) is considered to be very narrow, if any [1, 5, 7]. In the ternary Al-Fe-Ni system, the solubility of Fe in the Al-richest phase  $\text{NiAl}_3$  is 4 at%, while that in  $\text{Ni}_2\text{Al}_3$  is 2 at% [7].

The ternary intermetallic compound  $\text{FeNiAl}_9$  (9.1 at% Fe, 9.1 at% Ni, 81.8 at% Al) is formed at  $809^{\circ}\text{C}$  according to the peritectic reaction between the liquid phase  $L_1$  (87.06 at% Al, 2.11 at% Fe, 10.83 at% Ni),  $\text{FeAl}_3$  and  $\text{NiAl}_3$  [7]:



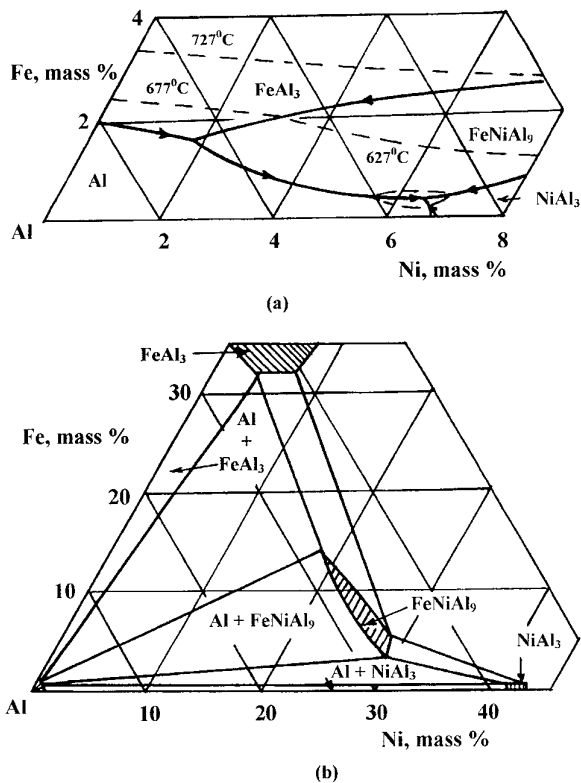


Figure 2 Projection of the liquidus surface on the concentration triangle and distribution of the phase fields in the solid state for Al-rich Al-Fe-Ni alloys [5].

Its range of homogeneity extends from about 3 to 11 at% Fe and from 7 to 17 at% Ni [7]. At 638°C, the eutectic reaction



takes place (see Fig. 2a). On cooling down the liquid  $L_2$  (96.72 at% Al, 0.105 at% Fe, 3.174 at% Ni), the eutectic mixture consisting of the aluminium solid solution  $\langle \text{Al} \rangle$ ,  $\text{NiAl}_3$  and  $\text{FeNiAl}_9$  is formed.

### 3.2. Morphology, microhardness and phase composition of intermetallic layers in the case of saturated aluminium melts

#### 3.2.1. Morphology and microhardness

Typical microstructures of the alloy-aluminium transition zones of the Al/(Fe-Ni) specimens obtained under the same conditions (temperature = 700°C, dipping time = 3600 sec, saturated aluminium melts) are shown in Fig. 3. The intermetallic layer,  $80 \pm 10 \mu\text{m}$  thick, grown between a 90 mass% Fe-10 mass% Ni alloy and the aluminium melt, saturated with the alloy constituents, seems to be one-phase (Fig. 3a). At a more close examination, however, it could be noticed that its crystals were not uniform in colour, some of them being a little darker than the others. Wherever the cracks were not too numerous, two separate sublayers could be distinguished. The sublayer adjacent to the alloy base was a little lighter in colour than that bordering with the aluminium matrix. Chemical compositions

of the sublayers were distinctly different (see the next section).

Microhardness,  $\text{HV}_{50}$ , was found to be 2.0 GPa for the Fe-Ni alloy base, 9.3 GPa for the intermetallic layer and 0.5 GPa for the aluminium matrix. The relative error of its measurement was around 10%.

Layer cracking appears to be a result of a few causes. The first is the difference in thermal expansion coefficients of interacting phases. The coefficient of thermal expansion is  $22.9 \times 10^{-6} \text{ m m}^{-1} \text{ K}^{-1}$  for aluminium,  $11.9 \times 10^{-6} \text{ m m}^{-1} \text{ K}^{-1}$  for iron,  $13.4 \times 10^{-6} \text{ m m}^{-1} \text{ K}^{-1}$  for nickel and  $15.2 \times 10^{-6} \text{ m m}^{-1} \text{ K}^{-1}$  for  $\text{FeAl}_3$  [5]. Due to this difference, significant lateral displacement of the phases occurs if the temperature changes. As in massive specimens these are not free either to move relative to each other or to bend, great mechanical stresses arisen cause brittle intermetallic layers to crack. Clearly, the cracks due to this cause occur mainly during cooling the Al/(Fe-Ni) specimens from the experiment temperature to room temperature.

The second is the volume effect associated with the formation of an intermetallic compound. In most cases, the volume of reaction products formed is not equal to the volume of reactants used. For example, in the case of  $\text{FeAl}_3$  the relative volume decrease is about 3%. Note that the cracks due to volume changes occur in the course of layer growth.

Though often invoked, the Kirkendall effect (see, for example [8]) appears to play an insignificant role, if any, in crack occurrence. The flow of vacancies due to this effect seems to be negligible to cause the appearance of macroscopic cracks or voids in growing intermetallic layers. This question was discussed in more detail elsewhere [9].

The intermetallic layer,  $90 \pm 10 \mu\text{m}$  thick, at the interface between a 75 mass% Fe-25 mass% Ni alloy and the aluminium melt, saturated with the alloy constituents, is one-phase (Fig. 3b). Elongated crystals of another phase, seen in the microstructure, were evidently formed from the melt during cooling. Microhardness value is 2.5 GPa for the alloy base, 7.6 GPa for the intermetallic layer and 0.7 GPa for the aluminium matrix.

Two intermetallic layers are observed between a 50 mass% Fe-50 mass% Ni alloy and the aluminium melt, saturated with the alloy constituents (Fig. 3c). The layer adjacent to the alloy base is only about  $8 \mu\text{m}$  thick. The much thicker layer bordering with the aluminium matrix tends to destroy. Its microhardness is 6.2 GPa. The microhardness of the alloy base is 2.1 GPa and that of the aluminium matrix is 0.7 GPa.

A tendency to destroying is more pronounced in the case of an intermetallic layer between a 25 mass% Fe-75 mass% Ni alloy and the aluminium melt, saturated with the alloy constituents (Fig. 3d). As seen, relatively large intermetallic grains were separated from the alloy base and passed into the liquid phase. Microhardness values are 2.3 GPa for the alloy base, 5.3 GPa for the intermetallic grains and 0.7 GPa for the aluminium matrix.

Unlike to preceding cases, the broad fine-grained two-phase zone, 2 mm thick, is formed at the interface

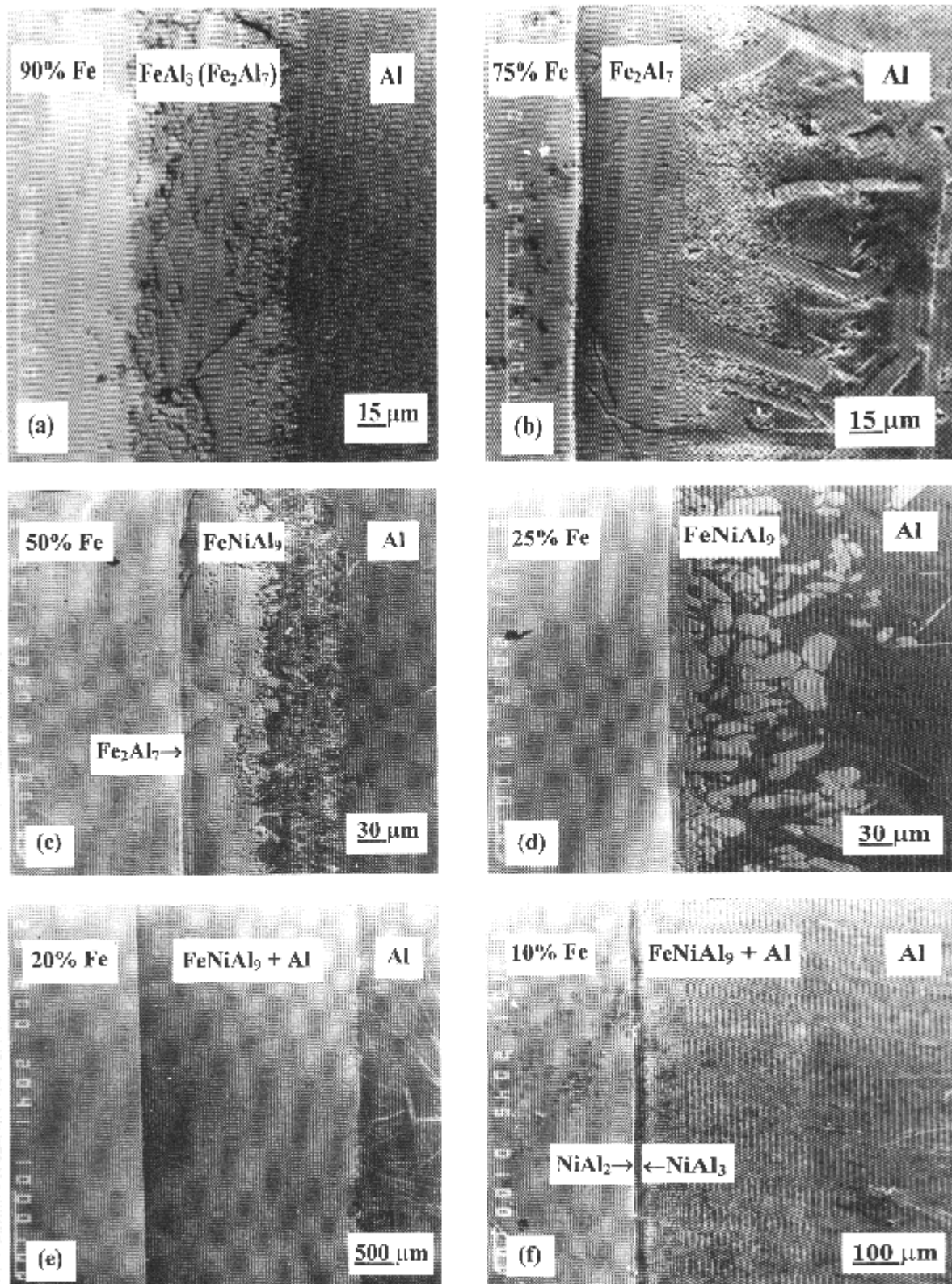


Figure 3 Backscattered electron compositional image of the Fe-Ni alloy and the aluminium melt, saturated with the alloy constituents. Dipping time = 3600 sec. The content of iron in Fe-Ni alloys is expressed in mass%.

between a 20 mass% Fe-80 mass% Ni alloy and the saturated aluminium melt (Fig. 3e). The same applies to a 15 mass% Fe-85 mass% Ni alloy, the thickness of the two-phase zone being 1.7 mm. One of the phases is dominant in the two-phase zone. Its fine crystals

form a framework whose pores are filled with another phase. Clearly, no microhardness measurements could be carried out in two-phase zones due to the irregular shape of indentations. Microhardness is 2.4 GPa for the 20 mass% Fe-80 mass% Ni alloy base and 0.57 GPa for

the aluminium matrix. In the case of a 15 mass% Fe-85 mass% Ni alloy, corresponding values are 2.1 GPa and 0.74 GPa.

As seen in Fig. 3f, the most complicated microstructure is formed between a 10 mass% Fe-90 mass% Ni alloy and the aluminium melt saturated with the alloy constituents. The compact one-phase intermetallic layer adjacent to the alloy base is about 8  $\mu\text{m}$  thick. The next layer,  $20 \pm 5 \mu\text{m}$  thick, is also compact. Then, the broad (around 300  $\mu\text{m}$ ) two-phase zone is observed. Microhardness value is 1.9 GPa for the alloy base and 0.88 GPa for the aluminium matrix. Intermetallic layers were too thin to measure their microhardness.

### 3.2.2. Chemical composition

EPMA measurements were carried out in the alloy-aluminium transition zone at a certain step in the direction normal to layer interfaces. The results obtained in the case of a 90 mass% Fe-10 mass% Ni alloy are presented in Table I. It is seen that, firstly, aluminium only slightly, if at all, dissolves in the alloy base whose composition remains to be close to the initial nominal value. Secondly, two phases can be distinguished, differing by the contents of aluminium and nickel, the content of iron being approximately the same in both. The chemical composition of the first phase bordering with the alloy base well corresponds to the composition of the  $\text{FeAl}_3$  compound, in which  $5.5 \pm 0.5$  at% Ni is dissolved. The chemical composition of the second phase is close to the upper Al limit of the homogeneity range of the  $\text{Fe}_2\text{Al}_7$  compound, in which much less Ni (0.7 to 1.4 at%) is dissolved. Hence,  $\text{FeAl}_3$  and  $\text{Fe}_2\text{Al}_7$  appears to be two different, though very closely related, phases.

Note that, of 2.5 mass% Fe and 0.28 mass% Ni added initially to aluminium in order to obtain the saturated melt at 700°C, only 0.41 mass% (0.20 at%) Fe and 0.05 mass% (0.03 at%) Ni is retained in an aluminium solid solution during cooling down the aluminium melt. The remaining iron and nickel react with aluminium to form a eutectic and intermetallic grains distributed at random in the aluminium matrix.

In the case of a 75 mass% Fe-25 mass% Ni alloy (saturated aluminium melt, dipping time 3600 and 900 sec), no formation of  $\text{FeAl}_3$  was observed. The intermetallic layer consisted of the  $\text{Fe}_2\text{Al}_7$  phase. Its composition ranged from 76.2 to 79.8 at% Al, the content of Ni being 2.5 to 4.8 at%.

No noticeable Al content was detected in the alloy base at a distance of 5 to 50  $\mu\text{m}$  away from the intermetallic-alloy interface. It is not, however, evidence for the lack of Al solubility in this and other Fe-Ni alloys investigated. Rather, all the aluminium atoms, diffusing through the bulk of growing compound layers, are spent in the formation of these layers [9]. No aluminium atoms are therefore available for the formation of a solid solution in the Fe-Ni alloy base (for more detail, see for example Ref. 9).

The contents of iron and nickel in the aluminium solid solution were around 1.30 mass% (0.63 at%) Fe and 0.47 mass% (0.22 at%) Ni. Note that initially 2.5

mass% Fe and 0.86 mass% Ni were added to aluminium to obtain the saturated melt. Thus, about half of these quantities could be retained in the supersaturated Al solid solution during cooling down the aluminium melt. Some of the elongated crystals, seen in the aluminium matrix (Fig. 3b), were found to be the  $\text{FeAl}_3$  phase while the others the  $\text{Fe}_2\text{Al}_7$  phase.

The ternary  $\text{FeNiAl}_9$  compound is dominant at the interface between a 50 mass% Fe-50 mass% Ni alloy and the aluminium melt, saturated with the alloy constituents (see Fig. 3c). The  $\text{Fe}_2\text{Al}_7$  compound only exists as a very thin layer (around 8  $\mu\text{m}$ ).

The chemical composition of  $\text{FeNiAl}_9$  ranged across the layer thickness from 81.5 at% (67.9 mass%) Al, 14.5 at% (24.9 mass%) Fe and 4.0 at% (7.2 mass%) Ni to 83.6 at% (70.5 mass%) Al, 8.7 at% (16.0 mass%) Fe and 7.7 at% (13.5 mass%) Ni. These values agree fairly well with the data known from the Al-Fe-Ni ternary phase diagram. The chemical composition of the  $\text{Fe}_2\text{Al}_7$  layer was 77.7 at% (62.3 mass%) Al, 14.7 at% (24.4 mass%) Fe and 7.6 at% (13.3 mass%) Ni at a distance of 2  $\mu\text{m}$  away from the alloy- $\text{Fe}_2\text{Al}_7$  interface and 79.7 at% (65.1 mass%) Al, 13.6 at% (22.9 mass%) Fe and 6.7 at% (12.0 mass%) Ni at a distance of 2  $\mu\text{m}$  away from the  $\text{Fe}_2\text{Al}_7$ - $\text{FeNiAl}_9$  interface.

Besides the  $\text{FeNiAl}_9$  compound layer, seen in Fig. 3d, two more phases were revealed at the interface between a 25 mass% Fe-75 mass% Ni alloy and the aluminium melt, saturated with the alloy constituents. At a smaller dipping time of 900 sec, cracking was not so pronounced as at 3600 sec, and the layers adjacent to the alloy base could be investigated by EPMA. The first measurement was carried out at a distance of 2.5  $\mu\text{m}$  away from the alloy-intermetallic interface, while the other measurements were made at a step of 2.5  $\mu\text{m}$  towards the aluminium matrix. The following set of aluminium, iron and nickel contents (at%) was obtained (Camebax SX50):

Al	66.4	67.5	67.7	70.4	75.6	75.6	81.3	82.0	82.9
Fe	7.5	8.1	9.5	9.2	6.9	6.6	5.4	6.0	7.1
Ni	26.1	24.4	22.8	20.4	17.5	17.8	13.3	12.0	10.0

It is seen that the first four points are close to the composition of a ternary solid solution based on the  $\text{NiAl}_2$  compound (33.3 at% Ni, 66.7 at% Al). However, such a phase does not exist according to the Al-Ni and Al-Fe-Ni equilibrium phase diagrams, the Ni-enriched phase next to  $\text{NiAl}_3$  being  $\text{Ni}_2\text{Al}_3$  [5–7]. As the Al content in the intermetallic layer under consideration far exceeds the upper limit of the homogeneity range of the  $\text{Ni}_2\text{Al}_3$  phase (63.7 at% Al [1] or 63.0 at% Al [7]), the phase grown can hardly be regarded as  $\text{Ni}_2\text{Al}_3$ . The next two points clearly belong to the  $\text{NiAl}_3$  phase, in which about 7 at% Fe is dissolved. The last three points are in accordance with the composition  $\text{FeNiAl}_9$ .

This specimen was remeasured with the help of another microanalyser (Superprobe 733). Similar results were obtained. For example, five measurements in the  $\text{NiAl}_2$  layer at a step of 1.5  $\mu\text{m}$  gave the following contents of the elements (at%):

TABLE I Data of electron probe microanalysis of the transition zone between a 90 mass% Fe-10 mass% Ni alloy and aluminium, saturated with the alloy constituents at 700°C. Drying time = 3600 sec

Distance from the alloy-intermetallic interface, $\mu\text{m}$	Phase	Content						Basic chemical formula
		Al		Fe		Ni		
		mass%	at%	mass%	at%	mass%	at%	
-10	Fe-Ni alloy	0.07	0.04	89.5	90.0	10.5	10.0	
10	Intermetallic	58.5	74.5	52.4	20.0	9.3	5.5	$\text{FeAl}_3$
20		58.7	74.9	57.0	19.1	10.3	6.0	
30		59.1	75.2	57.4	19.3	9.5	5.5	
40		63.2	78.1	54.5	20.5	2.5	1.1	$\text{Fe}_2\text{Al}_3$
50		64.5	79.1	53.0	19.5	2.5	1.4	
60		65.0	79.3	53.8	20.0	1.7	0.7	
70		65.4	79.7	52.8	19.3	1.8	1.0	
90	Al matrix	99.54	99.78	0.41	0.20	0.05	0.02	

Al	63.5	66.8	67.0	67.6	67.7
Fe	7.3	8.9	9.0	8.1	8.8
Ni	29.2	24.3	24.0	24.3	23.5

Therefore, no systematic instrumental error was possible. Thus, nine measurements carried out in the  $\text{NiAl}_2$  layer produce an average Al content of 67.2 at%, with the limiting values being 63.5 to 70.4 at%.

The broad two phase zones, formed at the interface between a 20 mass% Fe-80 mass% Ni alloy or a 15 mass% Fe-85 mass% Ni alloy and the saturated aluminium melts (Fig. 3c), consisted mainly of the  $\text{FeNiAl}_9$  compound and aluminium solid solutions. The  $\text{NiAl}_3$  inclusions were relatively seldom. The composition of  $\text{FeNiAl}_9$  grains changed from 80.6 at% (65.7 mass%) Al, 2.2 at% (3.7 mass%) Fe and 17.2 at% (30.6 mass%) Ni to 84.0 at% (70.9 mass%) Al, 3.5 at% (6.0 mass%) Fe and 12.5 at% (23.1 mass%) Ni. The content of nickel in the aluminium solid solutions was up to 3 at% (6.5 mass%), while that of iron did not exceed 0.2 at% (0.4 mass%).

The phase with a composition more close to  $\text{NiAl}_2$  rather than to  $\text{Ni}_2\text{Al}_3$  has also been found at the interface between a 10 mass% Fe-90 mass% Ni alloy and the aluminium melt, saturated with the alloy constituents, Table II. This phase formed a thin compact layer with even interfaces, adjacent to the Fe-Ni alloy base (see Fig. 3f). In this connection it seems relevant to remind that, in investigating the Al-Ni binary phase diagram, the formula  $\text{NiAl}_2$ , not  $\text{Ni}_2\text{Al}_3$ , was first ascribed to a phase enriched in nickel compared to  $\text{NiAl}_3$  (see Refs. [1] and [2]). That might probably be due to insufficiently pure materials used. The impurities could definitely cause a shift of intermetallic phase composition to higher Al content ( $\text{Ni}_2\text{Al}_3 \rightarrow \text{NiAl}_2$ ), as is seen from our data. Indeed, if the Fe content in the  $\text{NiAl}_2$  layer is around 8 : 1 at%, then the Al content varies across its thickness from 63.5 to 70.4 at%. However, if the Fe content lowers down to 3 or 4 at%, the Al content is 63.6 to 64.6 at%. The latter values are relatively close to the upper Al limit of the homogeneity range of the  $\text{Ni}_2\text{Al}_3$  phase. The other elements might perhaps produce a more pronounced effect. Clearly, this explanation is purely speculative. Unfortunately, due to small layer thicknesses, no structural studies could be carried

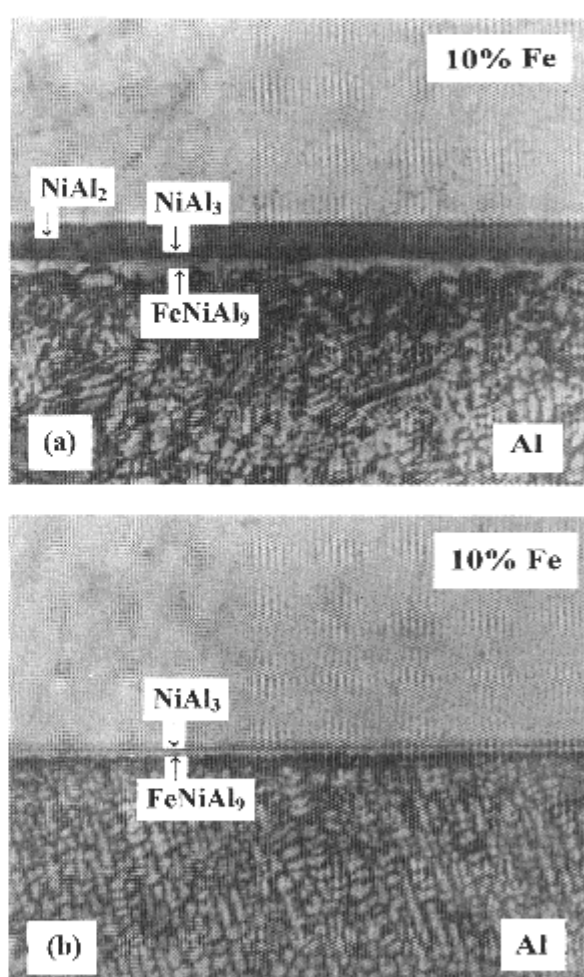


Figure 4 Optical micrograph of the transition zone between a 25 mass% Fe-75 mass% Ni alloy and aluminium. Initial liquid phase: (a) aluminium melt, saturated with the alloy constituents, (b) pure aluminium. Magnification  $\times 270$

out to show whether the crystal structures of  $\text{NiAl}_2$  and  $\text{Ni}_2\text{Al}_3$  were the same or different. Most likely, under non-equilibrium conditions the  $\text{NiAl}_2$  phase forms first, especially if a third component is present. As the system leads to equilibrium, it transforms into the  $\text{Ni}_2\text{Al}_3$  phase. Clearly, in reaction couples investigated the

TABLE II Data of electron probe microanalysis of the transition zone between a 10 mass% Fe-90 mass% Ni alloy and aluminium, saturated with the alloy constituents at 700°C. Dipping time = 3600 sec

Phase	Place of measurement	Content					
		Al		Fe		Ni	
		mass%	at%	mass%	at%	mass%	at%
Fe-Ni alloy	At a distance of $l = 50 \mu\text{m}$ away from the intermetallic-alloy interface	0.03	0.06	9.5	9.9	90.5	90.0
	$l = 10 \mu\text{m}$	0.05	0.12	9.6	10.0	90.3	89.8
	$l = 5 \mu\text{m}$	0.00	0.00	10.1	10.5	89.9	89.5
Thin intermetallic layer NiAl <sub>2</sub> near the Fe-Ni alloy base, Fig. 3f	In the middle of this layer;	44.6	63.6	5.9	4.0	49.5	32.4
	three points, 10 $\mu\text{m}$ away	45.7	64.6	4.7	3.2	49.6	32.2
	from each other	45.4	64.3	4.5	3.1	50.1	32.6
Next one-phase intermetallic layer NiAl <sub>3</sub>	Across this layer at a step of 3 $\mu\text{m}$ towards Al	58.0	75.0	1.9	1.2	40.1	23.8
		58.7	75.5	3.3	2.0	38.0	22.5
		60.1	76.5	4.5	2.8	35.4	20.7
		61.2	77.4	1.8	1.1	37.0	21.5
		61.5	77.6	2.7	1.7	35.8	20.7
		62.6	78.4	3.9	2.3	33.5	19.3
FeNiAl <sub>9</sub> grains of the two-phase zone	In the two-phase zone at a step of 30 $\mu\text{m}$ towards Al	68.8	82.6	6.0	3.5	25.2	13.9
		67.8	82.0	6.5	3.8	25.7	14.2
		70.7	83.9	6.0	3.5	23.3	12.6
		66.8	81.2	9.2	5.4	24.0	13.4
		72.0	84.7	6.8	3.9	21.2	11.4
		67.3	81.6	7.3	4.3	25.4	14.1
		69.9	83.3	6.6	3.8	23.5	12.9
		67.7	81.8	9.1	5.3	23.2	12.9
Al matrix (solid solution)	At a distance of $l = 50 \mu\text{m}$ away from the two-phase zone	92.1	96.2	0.0	0.0	7.9	3.8
		92.6	96.5	0.2	0.1	7.2	3.4
		93.1	96.7	0.2	0.1	6.7	3.2

intermetallic layer-growth conditions were far from the equilibrium state.

In contrast to the pure NiAl<sub>3</sub> phase, the ternary solid solution based on this phase exhibits a considerable range of homogeneity. Its composition was found to vary in growing intermetallic layers from 73.4 at% (56.3 mass%) Al, 7.5 at% (11.9 mass%) Fe and 19.1 at% (31.8 mass%) Ni to 79.7 at% (64.5 mass%) Al, 2.6 at% (4.4 mass%) Fe and 17.7 at% (31.1 mass%) Ni.

The composition of the FeNiAl<sub>9</sub> grains present in this specimen varied within the homogeneity range of the FeNiAl<sub>9</sub> phase from 81.2 at% (66.8 mass%) Al, 5.4 at% (9.3 mass%) Fe and 13.4 at% (23.9 mass%) Ni to 84.6 at% (72.0 mass%) Al, 3.9 at% (6.8 mass%) Fe and 11.5 at% (21.2 mass%) Ni. Of 8.1 mass% Ni and 0.51 mass% Fe added initially to aluminium in order to obtain the saturated melt at 700°C, up to 7.2 mass% (3.4 at%) Ni and 0.2 mass% (0.1 at%) Fe are retained in an aluminium solid solution formed during cooling down this melt to room temperature.

### 3.3. The effect of dissolution on the intermetallic layer formation

To show the influence of dissolution of the Fe-Ni alloy base into liquid aluminium on the layer formation, two sets of experiments were carried out using 75 mass% Fe-25 mass% Ni, 50 mass% Fe-50 mass%

Ni and 25 mass% Fe-75 mass% Ni alloys. In both sets the dipping time was 900 sec at 700°C. However, in the first set the saturated aluminium melts were used, while in the second the pure liquid aluminium was employed. In the latter case the Fe-Ni specimen was rotated at an angular speed of 24.0 rad sec<sup>-1</sup> to ensure its relatively rapid dissolution in liquid aluminium [1]. In the first set of experiments the total thickness of intermetallic layers formed at interfaces was three to five times greater than in the second, as shown in Fig. 4 for a 25 mass% Fe-75 mass% Ni alloy.

As seen in Fig. 4a, three layers (NiAl<sub>2</sub>, NiAl<sub>3</sub> and FeNiAl<sub>9</sub>) are present in the case of the saturated melt, whereas only two of them (NiAl<sub>3</sub> and FeNiAl<sub>9</sub>) survive under conditions of simultaneous dissolution in liquid aluminium (Fig. 4b), the total thickness of the layers being around 30  $\mu\text{m}$  and 10  $\mu\text{m}$ , respectively. When the pure liquid aluminium was employed, the content of aluminium in the NiAl<sub>3</sub> layer was close to the lower Al limit of the homogeneity range of the ternary solid solution based on the NiAl<sub>3</sub> phase (73.4 at% or 56.3 mass%). The FeNiAl<sub>9</sub> layer contained 87.7 at% (77.0 mass%) Al, 4.6 at% (8.3 mass%) Fe and 7.7 at% (14.7 mass%) Ni. The value 87.7 at% (77.0 mass%) is the upper Al limit of the homogeneity range of the FeNiAl<sub>9</sub> phase present as a separate layer in reaction couples.

The total thickness of the Fe<sub>2</sub>Al<sub>7</sub> and FeNiAl<sub>9</sub> intermetallic layers at the interface between a 50 mass% Fe-50 mass% Ni alloy and aluminium was 25 to 30 μm in the case of the saturated melt and 10 to 12 μm under conditions of simultaneous dissolution in pure liquid aluminium. In the latter case the Al content (76.7 at%) in the Fe<sub>2</sub>Al<sub>7</sub> layer was close to the lower Al limit of the homogeneity range of the Fe<sub>2</sub>Al<sub>7</sub> phase, while that in the FeNiAl<sub>9</sub> layer varied from 82.3 to 87.7 at%.

It is noteworthy that the intermetallic layer formed at the interface between a 75 mass% Fe-25 mass% Ni alloy and pure aluminium exhibited a composition range covering the ranges of homogeneity of both the FeAl<sub>3</sub> and Fe<sub>2</sub>Al<sub>7</sub> phases. Three EPMA measurements across its thickness (10 to 12 μm) at a step of 3 μm gave the following contents (at%):

Al	73.7	78.3	80.2
Fe	19.3	19.2	17.3
Ni	7.0	2.5	2.5

In the case of the saturated melt (in the absence of dissolution) the intermetallic layer thickness was 55 ± 5 μm, while its composition varied from 76.2 at% (60.3 mass%) Al, 17.5 at% (28.8 mass%) Fe and 6.3 at% (10.9 mass%) Ni to 78.4 at% (63.5 mass%) Al, 19.1 at% (32.0 mass%) Fe and 2.6 at% (4.5 mass%) Ni. This composition corresponds to the Fe<sub>2</sub>Al<sub>7</sub> phase.

#### 4. Conclusions

The FeAl<sub>3</sub> and Fe<sub>2</sub>Al<sub>7</sub> phases are formed at 700°C at the interface between a Fe-Ni alloy and the aluminium melt, saturated with the alloy constituents, if the Fe content of initial Fe-Ni alloys is less than or equal to 50 mass%. If this content is 50 mass% or more, the layers of the FeNiAl<sub>9</sub>, NiAl<sub>2</sub> and NiAl<sub>3</sub> phases are formed, with FeNiAl<sub>9</sub> being the dominant phase.

The FeAl<sub>3</sub>, Fe<sub>2</sub>Al<sub>7</sub>, NiAl<sub>2</sub> and NiAl<sub>3</sub> phases form one-phase layers, whereas the FeNiAl<sub>9</sub> phase can form either a one-phase layer or a two-phase zone with an aluminium solid solution. The formation of broad two-phase zones is only typical of Fe-Ni alloys containing 10 to 20 mass% Fe. The Al content of the ternary solid solutions based on these intermetallic phases varies in

growing layers in the following ranges:

1. FeAl<sub>3</sub>: 73.7 to 75.5 at%,
2. Fe<sub>2</sub>Al<sub>7</sub>: 76.2 to 79.8 at%,
3. FeNiAl<sub>9</sub>: 80.6 to 87.7 at%,
4. NiAl<sub>2</sub>: 63.5 to 70.4 at%,
5. NiAl<sub>3</sub>: 73.4 to 79.7 at%.

The Fe : Ni ratio of the intermetallic phases present in growing layers is strongly dependent upon the composition of initial Fe-Ni alloys. In some cases, this ratio exceeds the limits predicted from the Al-Fe-Ni equilibrium diagram.

Dissolution of the Fe-Ni alloy base into pure liquid aluminium causes a great decrease (a few times) of the thicknesses of intermetallic layers compared to the case of the saturated melt (in the absence of dissolution). Besides, even the number of growing layers can be altered. In studying the intermetallic layer-growth kinetics, the degree of saturation of a liquid metal with the alloy constituents should therefore be taken into account.

#### References

1. V. I. DYBKOV, *J. Mater. Sci.* **28** (1993) 6371.
2. M. HANSEN, "Constitution of binary alloys" (McGraw-Hill, New York, 1958) pp. 90, 118.
3. A. E. VOL, "Struktura i svoystva binarnikh metallicheskih sistem, Vol. I" (Fizmatgiz, Moskva, 1959) pp. 217, 400 (in Russian).
4. T. B. MASSALSKI, J. L. MURRAY, L. H. BENNETT and H. BAKER (Eds.), "Binary alloy phase diagrams, Vol. I" (American Society for Metals, Metals Park, OH, 1986) pp. 111, 140.
5. L. F. MONDOLFO, "Aluminium Alloys: Structure and Properties" (Butterworths, London, 1976) p. 532.
6. M. KHAIDAR, C. H. ALLIBERT and J. DRIOLE, *Z. Metallkunde* **73** (1982) 433.
7. P. BUDBERG and A. PRINCE, in "Ternary Alloys: A Comprehensive Compendium of Evaluated Constitutional Data and Phase Diagrams, Vol. 5," edited by G. Petzow and G. Effenberg (VCH, Weinheim, 1991) p. 309.
8. W. SEITH, "Diffusion in Metallen" (Springer, Berlin, 1955) Ch. 9.
9. V. I. DYBKOV, "Growth Kinetics of Chemical Compound Layers" (Cambridge International Science Publishing, Cambridge, 1998) Ch. 5.

Received 27 July 1998

and accepted 30 September 1999